Above-surface neutralization of highly charged ions: The classical over-the-barrier model

Joachim Burgdörfer
Department of Physics, University of Tennessee, Knoxville, Tennessee 37996-1200 and Oak Ridge National Laboratory, Oak Ridge, Tennessee 37831-6377

Peter Lerner
Department of Physics, University of Tennessee, Knoxville, Tennessee 37996-1200

Fred W. Meyer
Oak Ridge National Laboratory, Oak Ridge, Tennessee 37831-6372
(Received 28 May 1991)

The neutralization of highly charged ions during interaction with metallic surfaces is accompanied by the ejection of a large number of secondary electrons. Recent experiments demonstrate two main contributions to this electron ejection process: one from the region below the surface and the second from the above-surface portion of the trajectory. We present a theoretical analysis of the neutralization dynamics above the surface, prior to impact, based on the classical over-the-barrier model. The theory incorporates resonant multielectron capture of conduction electrons, resonant loss into unoccupied states of the conduction band, and intra-atomic Auger deexcitation. The effective barrier potential includes quantum corrections to the classical image potential. The effect of below-barrier ("tunneling") transfer is investigated. The solution of a coupled system of rate equations allows the approximate determination of the n-shell populations, the projectile charge state, and the total number of Auger electrons. The calculation describes the transient formation of "hollow" atoms. We find satisfactory agreement with recent data for K Auger yields by Meyer *et al.* [Phys. Rev. Lett. **67**, 723 (1991)].

PACS number(s): 34.70.+e, 79.20.Nc, 79.90.+b

I. INTRODUCTION

The study of neutralization of ions impinging on surfaces can be traced back to the early days of quantum mechanics [1,2]. Major progress was made in the 1950s when Hagstrum [3,4] identified detailed mechanisms for so-called potential emission, or more specifically, electronic emission by Auger transitions near the surface. For singly charged ions, interatomic Auger transitions involving two electrons from the conduction band [Auger neutralization (AN)] was found to dominate. In this "two-center" Auger process, one electron from the conduction band undergoes a nonresonant charge transfer into an atomic state (mostly the ground state) of the impinging projectile, while a second conduction electron is ejected carrying away the excess energy. The resulting secondary-electron emission spectrum contains detailed information on the electron structure of the conduction band, particularly of the surface density of states.

For doubly charged ions, Hagstrum found an alternative neutralization channel to be increasingly important, namely, resonant capture (RC) of conduction electrons into excited states of the projectile followed by intra-atomic Auger deexcitation. In view of the characteristic length scales involved, the latter channel is expected to dominate with increasing charge q of the impinging ion.

The advent of high-current low-energy sources for highly charged ($q \gg 1$) ions has revitalized this field and has led to a detailed investigation of the neutralization dynamics in several laboratories [5–12]. The typical perpendicular velocities $v_\perp$ presently available are of the order of 10^{-2} to 10^{-1} a.u. For collisions at small grazing angles θ, the velocity parallel to the surface is smaller than the Fermi velocity $v_\parallel \leq v_F$, such that kinematic resonances [13] of Galilei shifted energy levels are not yet important.

The complexity of the process involving a large number of electrons makes the delineation of the dominant pathways for neutralization difficult. However, a considerable amount of information has become available with which to begin unraveling the puzzle. Delaunay *et al.* [14] observed the emission of an increasing number of mostly low-energy secondary electrons with increasing charge state and decreasing projectile speed, in qualitative agreement with the picture of resonant capture followed by sequential ("ladder") intra-atomic Auger emission [15]. De Zwart *et al.* [8] found evidence for a Doppler shift of high-energy Auger lines consistent with the emission of Auger electrons "on the way in." This means that the emission occurs in the projectile frame with velocity $\mathbf{v}$ unperturbed by large angle or multiple scattering inside the solid. It should be noted that the latter does not necessarily imply that the emission has occurred above the surface, but rather that the emission occurs prior to significant deflection inside the solid. Recent high-resolution x-ray spectra by Briand *et al.* [9] and Andrä *et al.* [10] provided clear evidence for the transient formation of "hollow atoms." Multielectron transfer into high-lying states of the projectile creates a multiply excited nearly neutral atom with empty or only

sparsely populated ("hollow") inner shells. Changes of satellite intensities [10] as a function of the angle of incidence (or $v_\perp$) as well as changes in position and shape of K_α and K_β lines [11] may indicate that the formation of such exotic states is, at least in part, a surface effect. Hollow atoms correspond to an extreme case of level inversion with stored energies in the keV range. There is obviously considerable interest in the extrapolation of hollow-atom formation under well controlled conditions for x-ray laser applications.

The "ladder" model for above-surface neutralization faces, however, a fundamental "bottleneck" problem. Characteristic Auger rates are by far too slow to allow for the relaxation of the charge cloud to the states observed in the experiment. This suggests either a dramatic increase of intra-atomic Auger rates near the surface from their free-atom value or the coexistence of several different neutralization channels.

The fact that several pathways to neutralization may contribute simultaneously was recently demonstrated by Folkerts and Morgenstern [16], who measured simultaneously the *KLL* and the *LMM* Auger emission. From both the relative magnitude and the different $v_\perp$ dependence of the two intensities it became apparent that the *LMM* Auger transition is not always the precursor of a *KLL* transition as implied by the ladder model. The authors concluded, therefore, that additional "side feeding" of the *L* shell must provide a major contribution to neutralization. Most recently, Meyer *et al.* [17] achieved an experimental separation of different components of the *K* Auger spectrum for 60-keV N^{6+} impinging on a gold surface. At very small grazing angles $\theta = 0.5°$, they observed on top of a broad Auger peak a narrower component shifted in energy. Using the Marlowe simulation code they were able to identify the broad component as the *subsurface* component the *K* Auger emission while the narrow component was ascribed to *above-surface* Auger emission. The latter data allow a quantitative test for models of the neutralization dynamics above the surface.

In the following we present a theoretical description of the *above-surface* charge exchange and relaxation process. Our approach is modeled after the classical over-the-barrier model (CBM) originally developed for one-electron capture into highly charged ions in ion-atom collisions by Ryufuku, Sasaki, and Watanabe [18] and later extended by Barany *et al.* [19] and Niehaus [20] to incorporate multielectron transfer. In spite of its simplicity, it provides a surprisingly good first-order approximation to cross sections for electron capture into highly charged ions in slow ion-atom collisions. Two circumstances contribute to its relative success: resonant capture into a highly ionized projectile involves final states with high principal quantum numbers $n \gg 1$ for which, in line with the correspondence principle, a classical behavior is expected. Furthermore, the cross sections are large and of the order of the geometric size of the orbit involved. This, in turn, implies that dominant contributions to the cross section come from the classically allowed region. The transition takes place predominantly "over-the-barrier" between the potential wells of the target and the projectile rather than as a sub-barrier "tunneling" process. Clearly, finer details such as *l*-subshell cross sections are more difficult to describe [21]. The latter is easily understood by the fact that the dominant *l* values of the final states with $n \gg 1$ are not necessarily large.

In the following, we present an extension of the CBM to the analysis of the neutralization dynamics above the surface. The theory incorporates resonant multielectron capture of conduction electrons, resonant loss into unoccupied states of the conduction band, and intra-atomic Auger deexcitation. The effective barrier potential includes quantum corrections to the classical image potential. The effect of below-barrier ("tunneling") transfer is investigated. Modifications of atomic Auger rates near the surface are discussed and an additional relaxation mechanism, dielectric loss to the conduction band, is proposed. The model described the transient formation of "hollow" atoms. We find satisfactory agreement with recent data for *K* Auger yields by Meyer *et al.* [17].

The plan of the paper is as follows. The effective electronic potentials governing the charge transfer and the acceleration of charged particles near the surface are reviewed in Sec. II. In Sec. III, we introduce the system of coupled rate equations, which describe the evolution of the *n*-shell populations as the projectile approaches the surface. The approximations underlying the cross sections and transition probabilities for resonant electron capture into the projectile, resonant loss into unoccupied states of the conduction band, and the intra-atomic Auger rates entering the rate equations are discussed in Sec. IV. Numerical results for the *n*-shell populations prior to impact, the secondary-electron yield, and the *K* Auger rate for above-surface emission are given in Sec. V. Most of our numercial results presented in the following refer to the impact of hydrogenic nitrogen N^{6+} on a gold surface, which allows direct comparison with the data of Meyer *et al.* [17]. Atomic units are used unless otherwise stated.

II. SURFACE POTENTIALS

The interaction of a highly charged ion with surfaces is a true many-body problem. Even though we attempt a description for the electronic transfer processes within the framework of a mean-field or independent-particle model, collective effects due to the dynamical response of the conduction electrons have to be taken into account from the outset. The effective potentials governing both the motion of the ion and of the electrons contain collective screening and deviate from corresponding potentials for ion-atom collisions.

The classical interaction potential of a charged particle having charge *q* with a conducting surface is given by

$$V^I(z) = -\frac{q}{4z} \quad , \tag{1}$$

where z ($z > 0$) is the distance to the surface or, more precisely, to the image plane, which is slightly displaced relative to the topmost layer of atoms of the surface [22]. The classical expression (1) is only valid at large distances compared to the characteristic screening length for sur-

face plasmons,

$$\lambda_s = \omega_s / v_F \quad , \tag{2}$$

where ω_s is the surface-plasmon frequency and v_F is the Fermi velocity of the conduction band. Echenique *et al.* [23] have given an approximate expression for the quantum-mechanical self-image potential that accounts for the plasmon dispersion,

$$V^I(z) = -\frac{q\omega_s^2}{2}\int_0^\infty dp \frac{\exp(-2pz)}{\omega_s^2 + \alpha p + \beta p^2 + p^4/4} \tag{3a}$$

with $\alpha = \sqrt{3/5} v_F \omega_s$ and β is chosen such that the dispersion curve goes through the point (q_c, ω_c) where the bulk-plasmon dispersion curve enters the single-particle continuum. For gold, $\beta \simeq 0.35$. In the following, the conduction band is treated as a quasi-free-electron gas ("jellium"). For an electron with position vector $\mathbf{r}$ in the image field of another charged particle, the projectile with charge q located at the position $R\hat{\mathbf{z}}$ ($\hat{\mathbf{z}}$ is oriented along the surface normal), the corresponding quantum-mechanical image interaction is given by

$$V_{pe}^I(\mathbf{r}, R\hat{\mathbf{z}}) = q\omega_s^2 \int_0^\infty dp \frac{J_0(r_\parallel p) e^{-p(z+R)}}{\omega_s^2 + \alpha p + \beta p^2 + p^4/4} \tag{3b}$$

(J_0: Bessel function of zeroth order). Obviously, (3a) and (3b) tend to their respective classical values as $z \to \infty$. Equation (3) describes the static image potential. Dynamical screening is unimportant in the present context since the projectile velocity $v_p = (v_\perp^2 + v_\parallel^2)^{1/2} < v_F$. For fast ion-surface collisions at grazing incidence [24], dynamical generalizations of (3) should be used.

Both Eqs. (1) and (3) describe the collective *linear* response of the electron gas to a perturbing charge in front of the surface. For large q, nonlinear corrections to the response function become important [25]. An estimate for the critical distance $R_{\rm NL}$ of the onset of nonlinear response is given by

$$R_{\rm NL} \approx 2 r_s \sqrt{q} \quad , \tag{4}$$

where r_s is the one-electron radius of the electron gas. As will be discussed below, the q dependence of $R_{\rm NL}$ coincides with the one for the critical radius for resonant transfer [see Eq. (22)]. The coefficient in (4), however, turns out to be smaller than in (22) for most metals. Consequently, screening of the projectile by resonant transfer to the projectile sets in before nonlinear screening effects in the electron gas become important. This interplay between different screening mechanisms provides limited support for the use of linear-response theory.

The "active" electron to be transferred to the projectile experiences the interaction with its own image. The self-image potential represents one contribution to the work function W, or more precisely, to the background potential V_0 that confines the semi-infinite jellium. From investigations of localized surface states, it is known that the electronic self-image potential can be approximated by [26]

$$V_e^I(z) = -\frac{1}{4(z+z_0)} \quad , \tag{5}$$

where z_0 is chosen such that $V_e^I(z)$ is continuous across the jellium edge. As above, $V_e^I(z)$ approaches its classical value for $z \to \infty$.

The active electron at the position $\mathbf{r}$ in the presence of the ion at the position $R\hat{\mathbf{z}}$ is subject to the total potential

$$V(z) = V_e^I(z) + V_{pe}(|\mathbf{r} - R\hat{\mathbf{z}}|) + V_{pe}^I(\mathbf{r}, R\hat{\mathbf{z}}) \quad . \tag{6}$$

Equation (6) holds when both the electron and the projectile are above the surface, i.e., $z > 0$, $R > 0$. The effective interaction potential between the projectile and the electron is denoted by V_{pe}. For a bare nucleus or at large distances between the active electron and the projectile when its charge cloud can be treated as a point charge, V_{pe} is given by

$$V_{pe}(|\mathbf{r} - R\hat{\mathbf{z}}|) = \frac{-q}{|\mathbf{r} - R\hat{\mathbf{z}}|} \quad . \tag{7}$$

When the projectile-electron distance becomes comparable to the size of the charge cloud of electrons already bound to the nucleus (either carried into the collision or captured), we replace (7) by a Hartree-type static screening potential [27] ($x = |\mathbf{r} - R\hat{\mathbf{z}}|$),

$$V_{pe}(x) = -\frac{q_{\rm eff}(x)}{x} \quad , \tag{8}$$

with an effective charge self-consistently determined during the evolution of the system,

$$q_{\rm eff}(x) = q_{\rm asym} + \Delta q (1 + \Delta q^{1/3} x / R_c) e^{-2\Delta q^{1/3} x / R_c} \quad . \tag{9}$$

The analytic form of the screening function corresponds to that of a Hartree potential for a spherical $1s$-like charge distribution. In (9), the characteristic radius of the charge cloud is denoted by R_c and Δq is the charge of the cloud, i.e., the difference in charge between the inner pointlike charge q_i and the "outer" asymptotic charge $q_{\rm asym}$ of the projectile at large distances,

$$\Delta q = q_i - q_{\rm asym} \quad . \tag{10}$$

Obviously, $q_{\rm eff}(x)$ interpolates between q_i at $x = 0$ and $q_{\rm asym}$ for $x \to \infty$. In our numerical studies we will determine the q_i values according to Slater screening rules for "inner" screening. Accordingly, Eqs. (8) and (9) provide a description for "outer" screening during the charge-transfer process. The choice of the screening function is certainly not unique. However, as discussed below, we find no sensitive dependence on the choice of the screening potential.

The last term in (6), V_{pe}^I, describes the interaction between the electron and the image of the projectile. The value for the charge entering V_{pe}^I is not uniquely defined. One possible choice would be $q_{\rm eff}$ [Eq. (9)]. Noting, however, that the image charge is delocalized on the surface, the asymptotic charge of the charge cloud, $q_{\rm asym}$, is preferable. This follows from the observation that R_c is of the order of the distance of the projectile from the surface, R, and that, according to classical image charge

theory, a disk of the conducting surface with radius R contains only ≈ 0.3 of the total displacement charge q. Accordingly, the charge seen in the surface plane at large distances from the projectile determines the strength of the image interaction.

Finally, the interaction potential governing the acceleration of the projectile ion towards the surface reads

$$V_p(R) = q_{\text{asym}} V^I(R) \quad . \tag{11}$$

with the image potential V^I for the charge q_{asym} calculated from Eq. (3a) or (1). We note that q_{asym} will become R dependent due to the electronic transfer processes proceeding during the approach towards the surface.

Figure 1 displays the contours of the potential distribution for an electron moving in the fields of a charge of $q(=q_{\text{asym}})=6$, as given by Eq. (6). Several important features are noteworthy. At a distance of a few atomic units above the surface, a saddle develops that will provide a major pathway for resonant capture at large projectile-surface distances R. Near the saddle the contour corresponding to the Fermi energy ε_F delineates the "pass" through which capture proceeds. The width of the pass is small compared to R unless the projectile is in close proximity to the surface. This observation implies two consequences. The charge transfer proceeds in an approximately collinear geometry, which allows an approximate one-dimensional treatment with the coordinate along the surface normal, $\hat{z}$, as the reaction coordinate. Furthermore, the initial angular momentum l of the captured electron will be small: The outer turning point of orbits with low l or large eccentricities ($\epsilon \sim 1$) has, within a given n manifold, the largest distance from the nucleus and will therefore reach the region of the saddle first as the projectile approaches the surface. In addition, the impact parameters associated with the motion through the saddle are small. The subsequent electron-electron interaction will then lead to perturbation of this l distribution and to l mixing.

The structure of the potential surface (Fig. 1) is independent of the details of the model potentials entering Eq. (6). Numerical values near the saddle, the region most important for resonant charge transfer, are, however, sensitively dependent on the input potential. Figure 2 shows the electronic potential curve [Eq. (6)] along the surface-projectile axis for a bare projectile $q_{\text{asym}}=q_i=6$ using the classical [Eq. (1)] and quantum-mechanical expression [Eq. (3)] of the projectile image potential. While the position of the saddle is essentially unchanged, the height is reduced. The change of the barrier height can be easily understood: the incomplete quantum-mechanical screening near the surface reduces the repulsive interaction between the electron and the projectile image, thereby lowering the potential barrier. We note parenthetically that for semiconductor targets in comparison to that for metals, the potential barrier would be lowered. The effect of the saddle potential on the neutralization dynamics will be discussed in Sec. V.

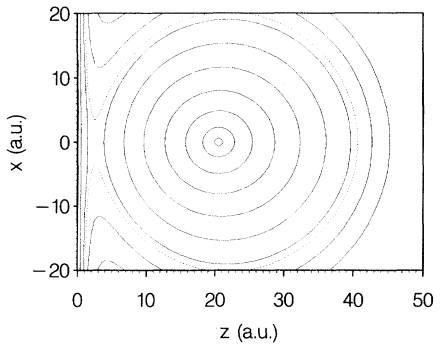

FIG. 1. Potential surface for an electron in the field of a N^{6+} ion at a distance $R=20.5$ a.u. from a gold surface; — — —, contour corresponding to the energy $\varepsilon=-0.17$.

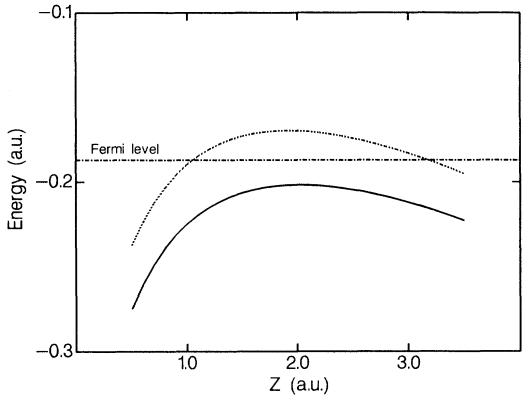

FIG. 2. Total electronic potential [Eq. (6)] near the saddle point for a N^{6+} ion at a distance of $R=18$ a.u. near a gold surface, including ——, quantum image potential [Eq. (3)] and — — —, asymptotic classical image potential [Eq. (1)].

III. THE RATE EQUATIONS

As the projectile ion approaches the surface, electrons are transferred resonantly from the surface to the projectile. At the same time, the reverse process becomes possible: electrons captured previously leak out across the saddle back into the solid provided that the final state is not forbidden by Pauli blocking. The near-resonant character follows from the fact that an electron moving in the potential [Eq. (6)] conserves its single-particle energy. Energy dissipation becomes possible if the potential fluctuations occur on a time scale comparable to the transit time of the electron (e.g., due to electron-electron scattering). In addition, as the number of electrons increases, intra-atomic Auger deexcitation sets in. In order to simulate this fairly complex array of processes, an n-electron classical trajectory Monte Carlo calculation (nCTMC) [28,29] could provide, within the limitations of classical dynamics, an adequate description. Major obstacles, however, make this approach difficult to apply. Apart from the large number of electrons to be treated and the associated large amount of CPU time necessary to accumulate sufficient statistics, the treatment of electron-electron collisions and of the Auger process

within the nCTMC is an unresolved problem. As is well known, classical two-electron systems (with the notable exception of helium [30,31]) are unstable, i.e., their probability of autoionization is unity. The quantum suppression of the classical instability against autoionization is not easily incorporated into a CTMC scheme.

In the following we use a much simpler approach in terms of coupled rate equations in which cross sections and rates for capture, loss, and deexcitation enter. The latter are modeled after the classical over-the-barrier model [18] and its generalizations [19–21]. Since in the CBM electrons move in a time-dependent mean field of surrounding charges, fluctuations and correlated charge-transfer events are neglected from the outset.

In the following we will study the set of coupled equations for the population P_n of the nth shell of the projectile as a function of the distance R of the projectile from the surface that reads

$$v_\perp(R)\frac{d}{dR}P_n(R)=I_n^C(R)-I_n^L(R)P_n(R) +\tfrac{1}{2}\sum_{n'>n}A_{n,n'}P_{n'}^2(R) -P_n^2(R)\sum_{n'<n}A_{n',n} \quad . \tag{12}$$

This set is augmented by the equation for the number of autoionized electrons $P_I(R)$,

$$v_\perp(R)\frac{d}{dR}P_I(R)=\tfrac{1}{2}\sum_{n'>n}A_{n,n'}P_{n'}^2(R) \quad . \tag{13}$$

Finally, the evolution of the perpendicular velocity of the approaching ion is described by Newton's equation of motion [see Eq. (11)]:

$$\frac{d}{dR}v_\perp(R)=\frac{1}{v_\perp(R)}\frac{d}{dR}V_p(R) \tag{14}$$

with

$$q_{\text{asym}}(R)=Z-\sum_n P_n(R) \tag{15}$$

(Z, nuclear charge of the projectile). The structure of this nonlinear system of equations (12)–(15) is as follows. We specify in Eq. (12) the population of the (multiply excited) bound states only in terms of their principal shells n. The assignment of l quantum numbers is, within the CBM, neither easily possible [21] nor physically meaningful near the surface because of strong mixing in l. The current of captured electrons, $I_n^C(R)$, plays the role of an inhomogeneous source term. An explicit expression for I_n^C within the CBM will be given below. One feature will be that I_n^C is nonzero only for a finite number of n quantum number ($n\le n_c$) determined by the over-the-barrier condition. Equation (12), therefore, becomes a system of equations of dimension n_c. The rate for the loss ("resonance ionization") into the unoccupied bound structure is denoted by $I_n^L(R)$ and will be discussed below. We note that both I_n^C and I_n^L are implicitly dependent on the vector $\{P_n(R)\}_{1\le n\le n_c}$ of occupation numbers. Finally, the remaining two terms in Eq. (12) describe the gain and loss due to autoionization events with rates $A_{n,n'}$. Since we will focus specifically on the "bottleneck problem" of the Auger rate limited neutralization process, we have included in (12) for simplicity only the subset of *fastest* decay channels that will come from electron pairs in the same shell. Rates for nonequivalent electrons ($A_{n_1,n_2',n_1,n_2'}$) could be incorporated if necessary. An estimate for $A_{n',n}$ will be discussed below.

Each Auger event leads to the emission of one electron per electron pair. The resulting population of continuum states due to "potential emission" is described by Eq. (13). In view of the simplicity of our approach, we have combined the spectrum of all Auger electrons to a single channel without attempting to keep track of the energy-differential spectrum. However, from the population numbers $P_n(R)$ we are still able to determine for low-lying n shells the number of Auger electrons for a given final n shell (in particular, of K Auger electrons). Finally, Eq. (14) describes the self-consistent coupling of the projectile motion in the multielectron transfer. The flow of the electron changes $q_{\text{asym}}(R)$ as a function of R rapidly on the time scale characteristic for the approach of the ion towards the surface. Therefore, the average number of transferred electrons at any given time determines the acceleration of the ion by its image charge. The use of classical dynamics for the ionic motion imposes a lower limit for $v_\perp$ for the validity of (14). We require that the De Broglie wavelength associated with the perpendicular speed is small compared to 1 a.u., i.e., $v_\perp \gtrsim \mu^{-1}$, where μ is the mass of the ion in atomic units. In the present case, $v_\perp \gtrsim 10^{-4}$ a.u.

The set of rate equations [Eqs. (12) and (13)] and Newton's equation of motion for the ion, Eq. (14), has to be integrated from infinity to the surface. Since they are adequate only for *above-surface processes,* we terminate the integration typically at a distance of one atomic radius above the surface. For close encounters with the topmost atomic layer as well as below-surface processes, the system of rate equations has to be modified.

The assignment of n "quantum numbers" designating the coupled channels in Eq. (12) requires the discretization of the classical energy continuum. For one-electron systems a straightforward method consists of forming energy bins determined by energy values corresponding to a half-integer quantum number ($n\pm\frac{1}{2}$). For the present problem of energy levels near the surface, this corresponds to the binning for the continuum of energies belonging to the energy level, ε_n,

$$-\frac{q^2}{2(n-\frac{1}{2})^2}+\frac{(q-\frac{1}{2})}{2R}\le\varepsilon_n(R)\le-\frac{q^2}{2(n+\frac{1}{2})^2}+\frac{(q-\frac{1}{2})}{2R} \quad . \tag{16}$$

In (16), the position of energy levels is modified by their image shift. We have used the asymptotic forms for large R for both the electronic self-image as well as the interaction with the projectile image charge. For small R the corresponding corrected expressions [see Eqs. (3) and (5)] should be used. The image interaction shifts the energy

levels upward as the ion approaches the surface. Therefore, the resonant n quantum number decreases as R becomes smaller.

For multielectron transfer a second and more important mechanism for the upward energy shift is the increasing screening of the core charge by previously captured electrons. The charge q in the Rydberg formula in (16) becomes dependent on n and on the vector of occupation numbers $\{P_n^{(R)}\}$ at a given R. We set

$$q_n(R)=Z-\sum_{n'\le n} P_{n'}(R)S_{n,n'} \ , \tag{17}$$

where $S_{n,n'}$ is the matrix of Slater screening values [32]. As discussed above, the image shift in (16) is more appropriately described by the asymptotic, i.e., n-independent but R-dependent charge $q_{\rm asym}(R)$.

IV. ESTIMATES FOR RATES

In this section we outline the approximations underlying the rates and cross sections entering Eqs. (12)–(15). We emphasize that improved rates could be easily implemented as input if available.

A. Electron capture

The crucial quantity for the neutralization dynamics is the current of captured electrons flowing into a given n shell, $I_n^C(R)$. According to the CBM, capture takes place when the saddle of the potential (Fig. 1), V_s, is lowered to below the threshold for an electron of energy ε to be transferred. Considering the beginning of the neutralization sequence, we find the critical distance R_c, where the first charge transfer takes place, from the condition

$$|V_s|=W \ , \tag{18}$$

where W is the work function of the surface and V_s is an implicit function of R.

From (16) we find in turn the critical value n_c,

$$n_c=\{\max n\,|\varepsilon_n(R_c)\le V_s\} \tag{19}$$

for the final n shell in which the first electron is captured. The latter is also the highest shell reached during the remainder of the neutralization sequence because screening and image shift of the levels will lower the n values. Equation (19) therefore determines the dimension of the system of Eqs. (12).

If one replaces the effective potentials by Coulomb potentials valid at large R, one can easily find approximate analytic expressions for the z coordinate of the saddle point. For $q\gg 1$ we have

$$z_s\simeq\frac{R}{\sqrt{8q+2}} \tag{20}$$

and the value of the potential at the saddle point

$$V_s=V(z_s)\simeq-\frac{1}{2R}\sqrt{8q+2} \ . \tag{21}$$

The critical distance R_c where the neutralization sequence begins is accordingly given by

$$R_c\simeq\frac{1}{2W}\sqrt{8q+2} \ . \tag{22}$$

The analytic form (22) differs from frequently used estimates [33,34] ($R_c\sim 2q+7$), which have been derived from an approximate treatment of the above-the-barrier process [33] and are linear in q. The latter leads for very large q to much larger critical distances than predicted by (22). It should be noted, however, that over the range of q values considered, the fit function suggested in Ref. [33] approximates (22) quite well (Fig. 3). Furthermore, using the effective potentials [Eqs. (3) and (5)] rather than the asymptotic Coulomb potential leaves the positions of the saddle essentially unchanged (Fig. 2) but alters the height of the potential and, hence, the critical distance R_c, shown in Fig. 3, by typically $\approx 10\%$.

The current can be written in terms of a geometric cross section of the "saddle" σ and the current density as

$$I_n^C(R)=\sigma(R)j_z^n(R) \ . \tag{23}$$

The current density along the surface normal is given by

$$j_z^n(R)=\tfrac{1}{4}\int_{\max[V_0,\varepsilon(n-1/2)]}^{\min[-W,\varepsilon(n+1/2)]} d\varepsilon' D(\varepsilon')T_{\rm cl}(\varepsilon',R) \times\sqrt{2|\varepsilon'+V_0|} \ , \tag{24}$$

where $D(\varepsilon)$ is the spectral density of states of the free-electron gas (or, in general of the surface band structure) and $T_{\rm cl}$ is the classical transmission function, which is a step function of the form

$$T_{\rm cl}(\varepsilon,R)=\Theta(R^*(\varepsilon)-R) \ . \tag{25}$$

In analogy to (22), $R^*(\varepsilon)$ is the critical distance below which for a given energy ε charge transfer proceeds over the barrier,

$$R^*(\varepsilon)=\frac{1}{2|\varepsilon|}\sqrt{8q_n(R)+2} \ . \tag{26}$$

The limits of the ε integral in (24) are determined by the

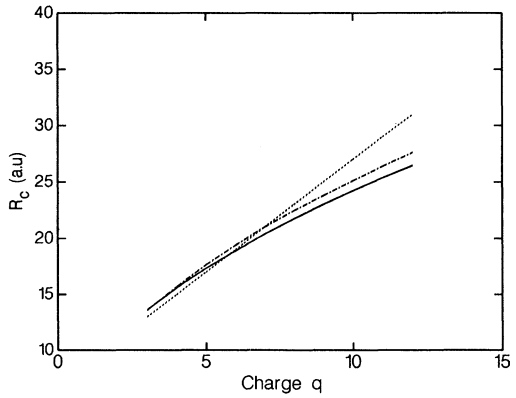

FIG. 3. Critical distance R_c for the onset of resonant neutralization: —·—·—·, quantum image potential [Eq. (3)]; ——, asymptotic classical image potential; — — —, fit formula $2q+7$ (Ref. [33]).

limits of the energy bins [Eq. (16)]. We note that for ions moving with a velocity parallel to the surface, $v_{\parallel}$, of the order of the Fermi velocity v_F, the spectral density of states corresponding to a Galilei shifted Fermi sphere should be used. By replacing the classical transmission function by a corresponding quantum-mechanical transmission function we will be able to assess the importance of subbarrier ("tunneling") processes. For the latter we will use the well-known Nordheim-Fowler formula for field ionization [35],

$$T_{\rm qm}(\varepsilon,R)=\exp\left[-\frac{2\sqrt{2}}{3}|\varepsilon|^{3/2}\frac{R^2}{q_n(R)}+\frac{1}{\sqrt{2\varepsilon_I}}\{\tfrac{1}{2}+\ln[4\sqrt{2}|\varepsilon|R/q_n(R)]\}\right] . \tag{27}$$

The geometric cross section for the saddle can be estimated as

$$\sigma(R)=\pi\{[R^*(\varepsilon)]^2-R^2\} . \tag{28}$$

Even though the geometric picture of the intersection of spherical ionic and planar surface equipotential lines underlying the estimate (28) is a drastic simplification (see Fig. 1), we find (28) to be in agreement with the numerically determined size of the saddle to within $\approx 30\%$. For subbarrier processes, $R > R^*(\varepsilon)$, and $\sigma(R)$ is no longer positive definite. In order to estimate contributions from electron tunneling, we replace (28) by

$$\sigma(R)\simeq\pi z_s^2 , \tag{29}$$

thereby assuming that the dominant contributions come from regions where the barrier is relatively low and that the width of this region is comparable to the distance of the saddle from the surface.

B. Electron loss

The estimate for the loss rate follows along similar considerations as for capture. An electron is considered to be lost when it hits the potential surface in the region of the saddle. The frequency of collisions with the wall can be estimated from the period of Coulomb orbits

$$\nu_n\simeq\frac{q_n^2(R)}{2\pi n^3} . \tag{30}$$

The probability for hitting the wall within the area of the saddle is of the order of

$$P(\varepsilon_n)\simeq[R^*(\varepsilon_n)-R]/R^*(\varepsilon_n) . \tag{31}$$

Loss into the solid can only take place if the energy of the level lies above the Fermi level. We find, therefore, for the loss rate

$$I_n^L(R)=\Theta(W+\varepsilon_n(R))P(\varepsilon_n(R))\nu_n . \tag{32}$$

Pauli blocking explicitly built into (32) does not pose a severe rate limiting factor. The reason is that the upward shift in energy [Eq. (16)] promotes the energy level very quickly to above the Fermi edge. Equation (32) loses its validity in the completely neutralized or even negatively charged ion ($q_n \lesssim 0$) since (30) can no longer be used to estimate the "bouncing" frequency. In the latter case, we estimate the rate from the average escape time of a free electron moving with kinetic energy $|\varepsilon_n|$ out of the sphere with radius R.

C. Auger deexcitation rates

The determination of Auger decay rates within the framework of classical dynamics is difficult due to the influence of quantum-mechanically forbidden decay channels. We use, therefore, input from quantum-mechanical calculations for Auger rates. Since we are interested in the exploration of the apparent incompatibility of time scales for the approach of the ion to the surface and for "ladder" Auger deexcitation, we focus here on the fastest subset of Auger rates. The latter occurs for electron pairs $(nlnl')$ in the same shell and in low l configurations. Furthermore, the decay rate is maximal for the largest final quantum number n' yielding a positive kinetic energy of the ejected electron, i.e, for the smallest allowed quantum jump $\Delta n = n - n'$ between the intial n and final n' quantum number of bound electrons. Using the Cowan code [36] calculating atomic Auger rates in vacuum we find for this set of Auger rates with $l=0$ and large n_i a simple scaling rule (Fig. 4) in atomic units,

$$A_{n,n'}=\frac{5.06\times10^{-3}}{|\Delta n|^{3.46}} . \tag{33}$$

Equation (33) is independent of the charge q, in agreement with known scaling properties [37]. It is interesting to note that Auger rates of Bhalla quoted by Briand *et al.* [9] agree with (33) to within a factor of approximately 2. Rates for low-lying states can be taken directly from the atomic structure codes [36,38]. The use of (33) in a classical nonlinear rate equation [Eqs. (12) and (13)] requires two corrections. The suppression of Auger decay due to partial population of the final n-shell population, i.e., due to reduction of the number of accessible final states, must be taken into account by an empirical reduction factor [38] approximately equal to $(1+1.5\times P_{n'})^{-1}$. The enhancement of Auger decay due to the multiple occupation of the initial shell is, within the framework of the kinetic equation [Eq. (12)], explicitly contained in the "collision" term of Eq. (12). However, since we do not keep track of subshell populations we must correct for distributions among (non)equivalent configurations. The

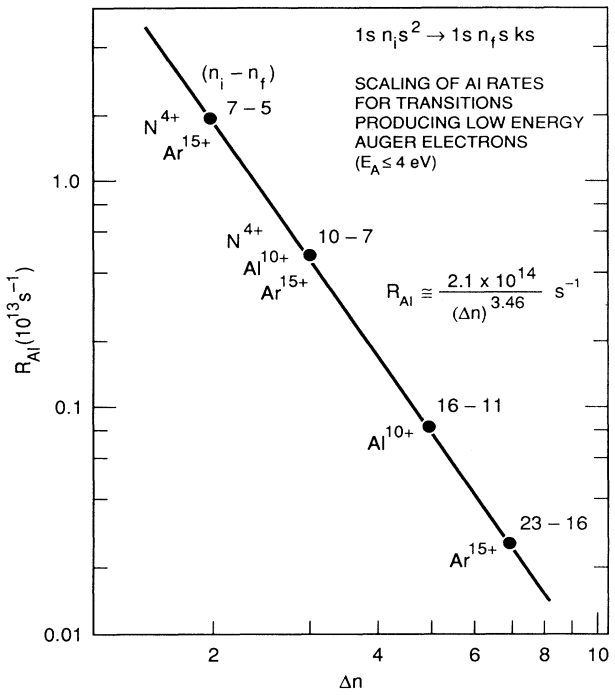

FIG. 4. Scaling behavior of Auger decay rates for highly excited ns^2 states for decay into final states with small kinetic energies (≤ 4 eV), calculated from the Cowan code (Ref. [36]).

correction factor approximatly equals 0.5 is chosen such as to reproduce the correct Auger rate for two equivalent electrons (e.g., ns^2) and for equal population in subshells of nonequivalent electrons (e.g., ns^1np^1).

The use of the Auger rates (33) for the decay of the n-shell population is, to a certain extent, an upper limit for atomic rates since the n-shell population will be spread over several angular momentum states. The approximation of the rates by their low l values is, however, justified in view of the saddle geometry (Fig. 1), which favors orbits with large eccentricities and hence low l. Furthermore, later steps of the ladder sequence will stay in the sector of terms with low total L if the first step was a low L state since $\Delta L = 0$ for dominant Coulomb allowed Auger transitions.

A conceptual difficulty results from the use of unperturbed atomic Auger rates itself. Near the surface atomic (or ionic) states are strongly perturbed. Two effects on the Auger rates should be distinguished: Stark mixing of initial and final states and changes in the threshold value Δn for the onset of autoionization. The former is due to the electric field generated by the image charge and gives rise to a redistribution of decay rates among substates but not to an overall increase of fastest rate among substates. Since Eq. (33) applies to the fastest rate within an n manifold, it is therefore still an acceptable first-order estimate. The second effect, however, may lead to a drastic change of the Auger rates for the initial stages of the cascade: unlike ions in free space the minimum energy transfer between the two electrons does not need to be sufficient for ejecting the electron *into the continuum*. Instead, any final state above the height of the saddle is sufficient for ejecting an electron into *unoccupied continuum states of the solid*. Since the final state of the mechanism proposed here is still a bound (negative energy) state relative to the vacuum level, we may call this modified Auger decay process *dielectronic loss* into the conduction band. This process contributes to the relaxation of multiply excited ions *near the surface* in complete analogy to ordinary Auger processes. Furthermore, since the initial state of the electron pair as well as the final state of the more deeply bound electron are identical to that for an ordinary Auger process, we can estimate the rate from extrapolating (33) to smaller Δn consistent with energy conservation for the above-barrier dielectronic loss process. Inclusion of this process permits us to estimate relaxation effects due to surface-specific decay processes. Dielectronic loss modifies the ladder deexcitation by adding additional steps of smaller size, thereby increasing the overall speed of the deexcitation. It should be noted that the dielectronic loss process operates only in the first few steps of the "decay ladder" since for low-lying n' ($n' \leq 4$ for N^{6+}) the smallest possible quantum jumps ($\Delta n = 1$, apart from Coster-Kronig intrashell transitions) are sufficiently large so as to directly ionize the ejected electron rather than to emit the electron into the band structure.

V. NUMERICAL RESULTS

In the following we present numerical results pertaining to the approach of N^{6+} ions towards a gold surface. Within the nearly-free-electron gas model, the gold surface is characterized by its work function [32,39] $W = 5.1$ eV, its Fermi energy $\varepsilon_F = 5.4$ eV, and its surface-plasmon frequency $\omega_s = 6.3$ eV. These values apply to the $6s$ band. One conceptual difficulty for the application of the jellium model results from the overlap of the $6s$ band with the completely filled band of $5d$ electrons in gold [40] displaying a rather complicated band structure including relativistic effects [41]. The latter cannot be represented by an electron-gas model and is not expected to contribute to above-surface charge-transfer processes because of its stronger localization.

We also note a considerable disagreement between the experimentally determined values of W for gold [32,42] of about $\approx 10\%$, which, apart from all other approximations, gives rise to a corresponding uncertainty in our result. Part of the discrepancy is due to the different crystallographic planes chosen as surfaces. However, as detailed below, the fundamental results concerning the characteristic time scales and the efficiency of the above-surface neutralization process remain unaffected by these uncertainties.

A. Formation of transient "hollow" atoms

As the N^{6+} ion approaches the surface, highly excited states with $n \lesssim n_c$ are resonantly populated. This leads to

the transient formation of hollow atoms (or ions) characterized by sparsely populated or empty inner shells and multiply occupied highly excited states. We emphasize the dynamical, transient nature of this process. With decreasing distance the n levels shift upward in energy [Eq. (16)] due to the image interaction and screening by electrons already transferred. Highly excited states continuously decay by resonant ionization and intra-atomic Auger processes. This results in a continuous shift of the population to lower n shells. Figure 5 illustrates the formation of hollow atoms. In order to accentuate the effect of different available interaction times, we have switched off the acceleration by the image interaction [Eq. (14)] in Fig. 5, i.e., the ion approaches the surface at a constant speed $v_\perp$. In this calculation, only standard Auger rates without modification by dielectronic loss have been used and the only classical above-barrier processes have been included according to Eq. (25). At $R=19$ a.u., just below R_c, the onset of resonant neutralization into $n=n_c=7$ becomes visible. At $R=15$ a.u. the growth of population of $n=5$ due to the first Auger cascade step can be observed. Even closer to the surface, at $R=10$ a.u., we find for $v_\perp=5\times10^{-3}$ a.u. and $v_\perp=9\times10^{-3}$ a.u. a nearly neutral hollow atom with, on the average, approximately five electrons in $n=7$, approximately one electron in $n=5$ and one K-shell electron carried into the surface collision. Only for the smallest speed, $v_\perp=1\times10^{-3}$ a.u., can a change of the K-shell population due to Auger processes be found. Here, the cascade population stretches from $n=5$ to $n=1$ with rapidly decreasing average occupation numbers. At the same time, increased screening shifts the resonant level towards $n=6$. The point to be noticed is that the time interval for the cascade starting at $n=7$ is insufficient to reach the K shell for the ions with $v_\perp\geq5\times10^{-3}$. The increased K-shell population for the smallest velocity is due to both the larger time interval available as well as due to the shift of the resonant level to $n=6$, which reduces the number of cascade steps and accelerates the cascade sequence.

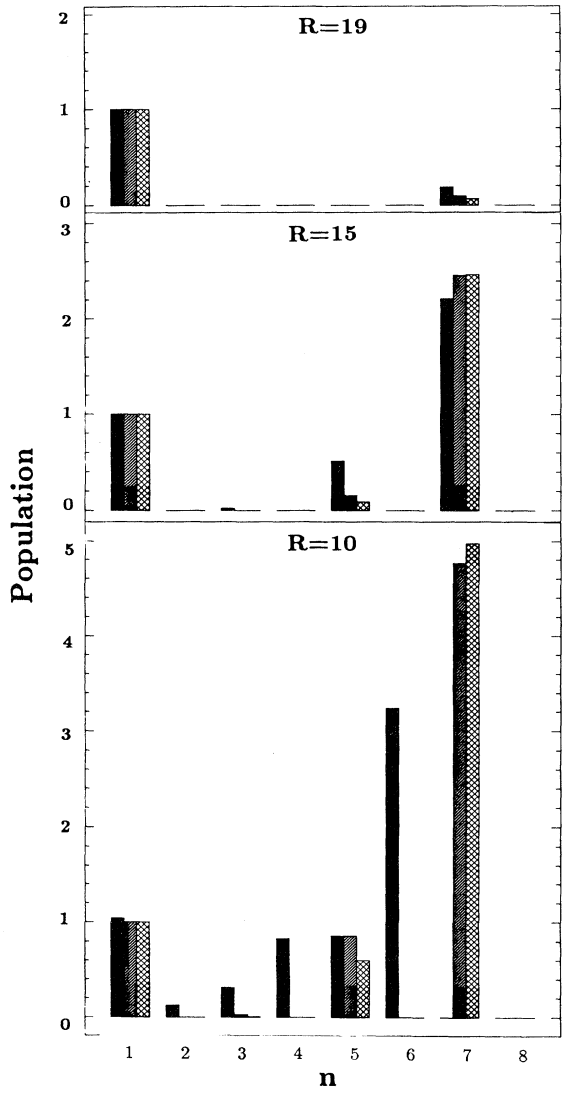

FIG. 5. Formation of hollow atoms near surfaces; occupation numbers of n shells for different distances from the surface; calculation for N^{6+} on gold for three different speeds (columns from left to right): $v_\perp=1\times10^{-3}$, 5×10^{-3}, 9×10^{-3}. Classical barrier transmission function [Eq. (25)]; image acceleration [Eq. (14)] switched off.

Quantum-mechanical subbarrier ("tunneling") processes are thought to be most important at large distances R when the resonant transfer is still classically forbidden. We have investigated the influence of tunneling on the formation of hollow atoms. Figure 6 shows the excited-state distribution for the same parameters as in Fig. 5 using, however, the quantum-mechanical transmission function (27) for distances $R>R^*(\varepsilon)$ where transfer is classically not allowed. It should be noted that the

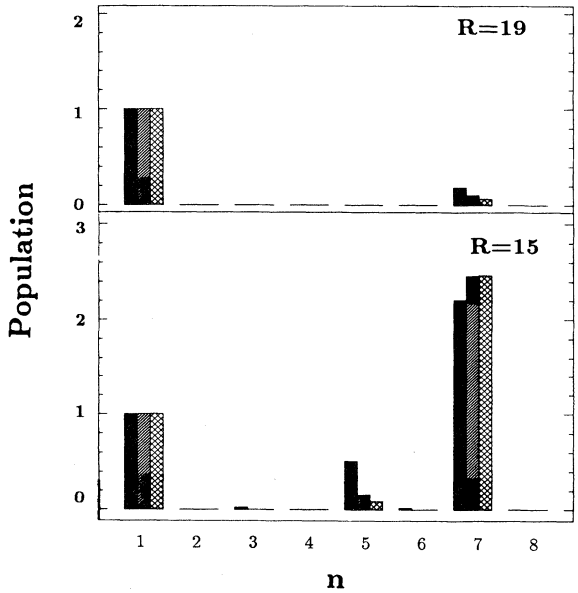

FIG. 6. Formation of hollow atoms near surface, parameters as in Fig. 5, however with a quantum-mechanical sub-barrier transmission function [Eq. (27)].

Nordheim-Fowler factor (27) for thick barrier penetration is not valid for $R < R^*(\varepsilon)$ for which we use (25) instead. The n-shell distribution is virtually unchanged as compared to the classical over-the-barrier distribution (Fig. 5). Obviously, tunneling processes are by far too slow to build up significant excited state population in the considered range of speeds $v_\perp$. Only for much smaller speeds, $v_\perp \ll 10^{-3}$ a.u., would the tunneling rates suffice to form hollow atoms (or ions) at distances $R > R_c$ larger than the critical radius for over-the-barrier transitions. For such small speeds ($v_\perp \lesssim 10^{-4}$ a.u.), however, the classical description of the ionic motion would break down. More importantly, the acceleration of the ion by the image interaction, neglected in the results of Figs. 5 and 6, renders this velocity range inaccessible.

B. K Auger yields

Since above the surface or, more precisely, at distances outside the range of two-center AN processes ($R \gtrsim 1.5$ a.u.) no direct charge transfer to the K shell of N is possible, the change of K-shell population gives directly the number of K Auger electrons emitted per ion. In Fig. 7 we present the K Auger yield as a function of the inverse normal projectile velocity $v_\perp^{-1}$, which is a measure for the interaction time, and a comparison with recent experimental data [17,43]. The hatched areas characterize a theoretical "error bar" and illustrate the uncertainty of the final results due to several model assumptions entering the classical over-the-barrier model.

The "error bar" is determined from a large number of calculations with different forms of the image potentials

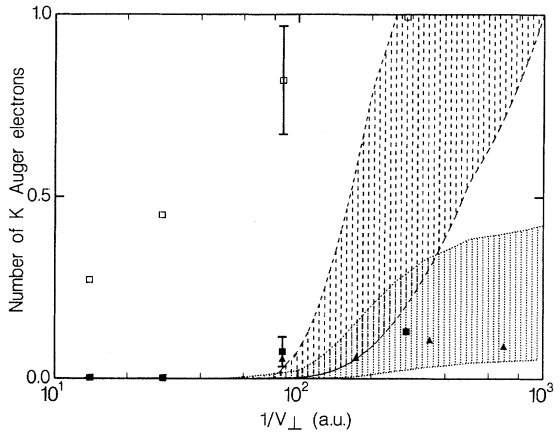

FIG. 7. Above-surface K Auger yield for an N^{6+} ion impinging on a gold surface as a function of inverse asymptotic perpendicular speed $v_\perp^{-1}$. Experiment (Refs. [17] and [43]): □, total K Auger yield; ■, above-surface yield; ▲, above-surface yield for Cu target. Theory: upper band, solution of the system of coupled rate equation without image acceleration; lower band, solution of the system of rate equations including image acceleration (see text).

[Eqs. (1) and (3)], different forms of the screening functions [Eqs. (8) and (17)], and different choices for the Auger rates. The results obtained incorporating these variations lie within the two "bands" displayed in Fig. 7. The two bands differ from each other in that for the upper band the acceleration of the ion by the image potential [Eq. (14)] was switched off while for the lower band the self-consistent coupling of the projectile motion to the neutralization process was taken into account.

The acceleration of the ion leads to a saturation of the K Auger yield for large $v_\perp^{-1}$ (or small $v_\perp$). The obvious reason is that no matter how small the *asymptotic* value of $v_\perp$ for the incident projectile is, the acceleration by the image potential limits the available interaction time above the surface and prevents in all cases considered the complete filling of the K shell. On the average, more than 0.5 K vacancies per ion will be carried into these collisions with the atomic surface or below-surface layers. We find that the suppression of K-shell filling depends on the details of the neutralization dynamics, which is coupled to the acceleration for the ion "on the way in."

The upper boundaries for each band correspond to the calculations incorporating the effectively enhanced Auger rates by inclusion of dielectronic loss into the conduction band and of the quantum-mechanical image potential [Eq. (3)], while the lower boundaries to the calculation using only standard Auger rates and the asymptotic classical expression for the image potential [Eq. (1)]. Both the incomplete quantum-mechanical screening of the projectile charge by surface plasmons and the dielectronic loss processes enhance the speed of the neutralization cascade. Nevertheless, even when the image acceleration is switched off, no appreciable K Auger emission takes place at speed $v_\perp > 10^{-2}$ a.u. This conclusion is obviously valid irrespective of the ambiguities associated with the treatment of such a complex multielectron transfer problem and confirms the conclusion of Ref. [17] that the K Auger intensity of the broad peak, also shown in Fig. 7, can be unambiguously associated with subsurface processes. On the other hand, the onset of the narrow peak at speeds $v_\perp \lesssim 10^{-2}$ is reproduced by all our calculations for the K Auger yields irrespective of the details of the model assumptions, thereby confirming its identification as the above-surface component.

Most remarkably, the experimental data [17,43] appear to show the saturation of the K Auger yield at low speeds $v_\perp$ in accordance with our calculations. While a direct comparison with these data is complicated by the fact that they pertain to a different (Cu) surface, they provide strong support that image acceleration indeed suppresses above-surface K-shell filling, which otherwise would take place within a relatively sharply defined velocity interval $2\times10^{-3} \le v_\perp \le 5\times10^{-3}$.

C. Total secondary-electron yield

From the solution of Eq. (13) we can directly infer the total secondary-electron yield ascribable to "potential" electron emission due to intra-atomic Auger processes. Several limitations on the validity of the results for total secondary-electron yields should be stressed. The calcu-

lations refer only to potential emission *above the surface.* Considering the large number of vacancies carried into the surface (see Sec. V B), a significant contribution to potential electron emission originates from below-surface processes. In fact, our calculations suggest that the latter provides the dominant contribution for $v_\perp > 10^{-2}$ a.u. Furthermore, the number of observed electrons is determined by the R-dependent solid angle for direct emission into the vacuum, together with the energy-dependent degree of reflection of the emission towards the surface. Any detailed estimate would require the knowledge of the energy-differential emission spectrum, which is beyond the scope of the present model. The solution of Eq. (13) refers to the total number of Auger events irrespective of the subsequent fate of the emitted electrons. Furthermore, when the hollow atom (Figs. 5 and 6) strikes the surface, another secondary-electron emission mechanism becomes operative: the outer shells of the hollow atoms get "peeled off" as a result of the dynamical screening inside the solid [44]. A fraction of these electrons will be emitted while the remaining fraction will occupy empty states of the conduction band. While our theoretical approach would permit the determination of the number of "peeled off" electrons, it does not provide an estimate for the fraction of backward-scattered electrons into vacuum. We have therefore omitted this contribution.

Our results (Fig. 8) clearly exhibit a strong correlation between the filling of the K shell and an avalanche of secondary electrons. When the K shell is almost completely filled (in simulations without image acceleration and $v_\perp \lesssim 5\times10^{-3}$ a.u.), typically ≈ 30 Auger electrons are emitted per ion. The latter can be easily understood from simple statistics. If p is the number of cascade steps, typically 2^p Auger processes are involved in the cascade resulting in a single KLL Auger event (provided sufficient potential energy is available). In the present case, $p \approx 5$ and $2^p \approx 32$. Conversely, when the majority of K vacancies survives (in the model calculations including image acceleration), a significantly reduced but still large number of Auger electrons (≈ 10) is emitted.

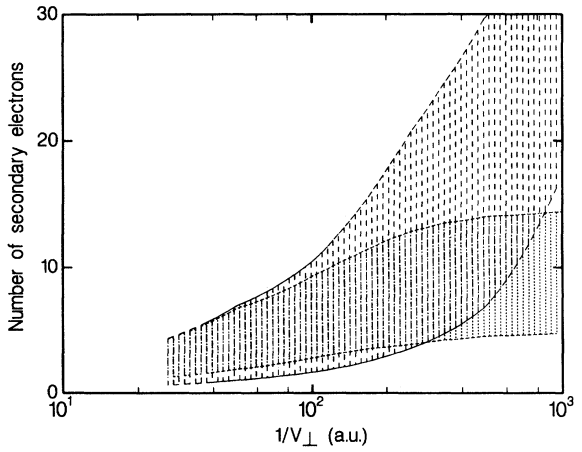

FIG. 8. Total number of Auger electrons per N^{6+} ion impinging on a gold surface as a function of the inverse asymptotic speed: upper band, solution of rate equation without image acceleration; lower band, solution of rate equations including image acceleration (see text).

While the present results pertain to the collision process $N^{6+} \rightarrow Au$, some tentative conclusion can be drawn for other studies of secondary-electron emissions as well. The number of observed secondary-electron emissions [14] for Ar^{q+} ions ($7 \le q \le 12$), while impressively large, is still significantly below the corresponding statistical estimate given above for a nearly completed neutralization and relaxation sequence. The latter clearly indicates that below-surface neutralization will account for a significant fraction of processes leading to the filling of the inner shells. This is consistent with the relatively large speeds $v_\perp \gtrsim 4\times10^{-2}$ a.u. realized in that experiment.

VI. CONCLUSIONS

The present above-the-barrier model for above-surface neutralization of highly charged ions provides, despite its inherent oversimplifications, realistic quantitative estimates for the characteristic time (velocity) scales as well as the efficiency of above-surface neutralization dynamics. Both the mean potentials governing the multielectron transfer and the Auger decay rates of the multiple excited states are not accurately known. It turns out, however, that despite these uncertainties the resulting neutralization dynamics is governed by a well-defined time scale. The model describes successfully the formation of transient hollow atoms. In the present collision system, $N^{6+} \rightarrow Au$ for $v_\perp > 10^{-2}$ a.u., the Auger relaxation remains incomplete, and essentially all K-shell vacancies are carried into the solid. For lower speeds, partial filling of the K vacancy becomes possible. The K Auger emission is, however, reduced by the image acceleration. The neutralization does not proceed fast enough and at sufficiently large distances so as to terminate the image acceleration at an early stage. Consequently, the effective speed for approaching the surface does not drop substantially below 10^{-2} a.u. and the ion carries a large fraction of K vacancies into the surface irrespective of the asymptotic speed $v_\perp$. These conclusions appear to be valid irrespective of the assumptions used in the solution of the set rate equations [Eqs. (12)–(14)]. We find satisfactory agreement with recent experimental data by Meyer *et al.* [17,43] for the above-surface component of the K Auger emission.

The total number of Auger electrons is found to be strongly correlated with the fraction of K-shell filling achieved in the neutralization sequence. For the nearly completely filled K shell, the total number of secondary electrons is approximately given by the statistical estimate (2^p, p is the number of steps of the relaxation sequence). For ions with a large fraction of K vacancies the total yield is substantially smaller. We point out that the avalanche of secondary electrons can be used as an independent test for the degree of above-surface neutralization and relaxation. If the yield lies significantly below the statistical estimate, the relaxation of the charge cloud occurs most likely in close collisions at the surface or inside the solid rather than above the surface. It should be

noted that in the latter case the approximate proportionality between total secondary-electron yield and the amount of potential energy [15] carried into the collision may still be preserved. Energy loss by multiple scattering of energetic electrons and ejection of additional electrons in a collision cascade may account for the required energy distribution over many electrons.

In closing we point to future directions: a treatment of the multielectron transfer process beyond the mean-field approach within the framework of either classical [45] or quantum N-body dynamics would be highly desirable. Of particular importance is the modification of the effective above-the-barrier electron flow due to correlated transfer processes. The latter could lead to either an enhancement or a decrease of the capture current, depending on the spatial separation of the two correlated electrons relative to the distance of the ion from the surface. Finally, a more complete description of the interaction of the highly charged ion surface requires treatment of processes occurring at the surfaces and inside the first few layers such as two-center Auger capture and ion-atom-like processes. Preliminary estimates indicate that the 5*d* level of gold will provide a major contribution to quansiresonant transfer during the penetration of the first few atomic layers.

ACKNOWLEDGMENTS

One of us (J.B.) acknowledges illuminating discussions with Norman Bardsley on the Nordheim-Fowler field-ionization theory. P.L. acknowledges financial support by the Science Alliance, University of Tennessee. This work was supported in part by the National Science Foundation and by the U.S. Department of Energy, Office of Basic Energy Sciences, Division of Chemical Sciences, under Contract No. DE-AC05-840R21400 with Martin Marietta Energy Systems, Inc.

[1] G. Holst and E. Oosterhuis, Physica **1**, 78 (1921).
[2] M. L. E. Oliphant, Proc. R. Soc. London **27**, 373 (1930).
[3] H. D. Hagstrum, Phys. Rev. **96**, 336 (1954).
[4] H. D. Hagstrum and G. Becker, Phys. Rev. B **8**, 107 (1973).
[5] E. D. Donets, Phys. Scr. **T3**, 11 (1983).
[6] M. Delaunay *et al.*, Nucl. Instrum. Methods B **23**, 177 (1987).
[7] F. W. Meyer, C. C. Havener, K. J. Snowden, S. H. Overbury, D. M. Zehner, and W. Heiland, Phys. Rev. A **35**, 3176 (1987).
[8] S. de Zwart *et al.*, Surf. Sci. **217**, 298 (1989).
[9] J. P. Briand *et al.*, Phys. Rev. Lett. **65**, 159 (1990).
[10] H. J. Andrä *et al.*, in Proceedings of the Vth International Conference on the Physics of Highly Charged Ions [Z. Phys. (to be published)]; J. J. Bonnet *et al.*, *ibid.*
[11] M. Schulz, C. Cocke, S. Hagmann, M. Stöckli, and H. Schmidt-Böcking, Phys. Rev. A **44**, 1653 (1991).
[12] R. Köhrbrück, D. Leller, F. Fremont, P. Roncin, K. Sommer, T. Zouros, J. Bleck-Neuhaus, and N. Stolterfoht, Nucl. Instrum. Methods B **56/57**, 219 (1991).
[13] J. Burgdörfer, E. Kupfer, and H. Gabriel, Phys. Rev A **35**, 4963 (1987), and references therein.
[14] M. Delaunay, M. Fehringer, R. Geller, D. Hitz, P. Varga, and H. Winter, Phys. Rev. B **35**, 4232 (1987).
[15] U. A. Arifov, E. S. Mukhamadiev, E. S. Parilis, and A. S. Pasuyk, Zh. Tekh. Fiz. **43**, 375 (1973) [U. A. Arifov, L. M. Kishinevskii, E. S. Mukhamadiev, and E. S. Parilis, Sov. J. Tech. Phys. **18**, 203 (1973)].
[16] L. Folkerts and R. Morgenstern, Europhys. Lett. **13**, 377 (1990).
[17] F. Meyer, S. Overbury, C. Havener, P. Zeijlmans van Emmichoven, and D. Zehner, Phys. Rev. Lett. **67**, 723 (1991).
[18] H. Ryufuku, K. Sasaki, and T. Watanabe, Phys. Rev. A **21**, 7451 (1980).
[19] A. Barany, G. Astner, H. Cederquist, H. Danared, S. Huldt, P. Hvelplund, A. Johnson, H. Knudsen, L. Liljeby, and K. Rensfelt, Nucl. Instrum. Methods B **9**, 397 (1985).
[20] A. Niehaus, J. Phys. B **19**, 2925 (1986).
[21] J. Burgdörfer, R. Morgenstern, and A. Niehaus, J. Phys. B **19**, L507 (1986); Nucl. Instrum. Methods B **23**, 120 (1987).
[22] N. Lang and W. Kohn, Phys. Rev. B **7**, 354 (1973).
[23] P. M. Echenique, R. H. Ritchie, N. Barberan, and J. Inkson, Phys. Rev. B **23**, 6486 (1981).
[24] See, e.g., K. Kimura, M. Hasegawa, and M. Mannami, Phys. Rev. B **36**, 7 (1987); H. Winter, R. Kirsch, J. Poizat, and J. Remillieux, Phys. Rev. A **43**, 1660 (1991).
[25] P. Appell, Nucl. Instrum. Methods B **23**, 242 (1987).
[26] G. Thörner and G. Borstel, App. Phys. A **41**, 99 (1986), and references therein.
[27] C. Joachain, *Quantum Collision Theory* (North-Holland, Amsterdam, 1975), p. 543.
[28] R. Abrines and I. C. Percival, Proc. Phys. Soc. London **88**, 861 (1966).
[29] R. E.Olson and A. Salop, Phys. Rev. A **16**, 531 (1977); R. E. Olson in *Electronic and Atomic Collisions,* edited by H. Gilbody, W. Newell, F. Read, and A. Smith (North-Holland, Amsterdam, 1988), p. 271.
[30] K. Richter and D. Wintgen, J. Phys. B **23**, 1197 (1990).
[31] J. Müller, J. Burgdörfer, and D. Noid (unpublished).
[32] See, e.g., T. Martin and W. Leonard, *Electrons and Crystals* (Brooks/Cole, Belmont, 1970).
[33] K. J. Snowdon, Nucl. Instrum. Methods B **34**, 309 (1988).
[34] H. Winter, in Proceedings of the Vth International Conference on the Physics of Highly Charged Ions (Ref. [10]).
[35] S. Flügge, *Rechenmethoden der Quantenmechanik* (Springer, Berlin, 1976).
[36] R. D. Cowan, *The Theory of Atomic Structure and Spectra* (University of California Press, Berkeley, 1981).
[37] L. Landau and L. Lifshitz, *Course of Theoretical Physics, Vol. III* (Pergamon, Oxford, 1979).
[38] P. Zeijlmans Van Emmichoven, C. Havener, and F. Meyer, Phys. Rev. A **43**, 1405 (1991).
[39] C. Kittel, *Introduction to Solid State Physics* (Wiley, New York, 1971).
[40] D. Shirley, Phys. Rev. B **5**, 4709 (1972).
[41] S. Kupratakuln, J. Phys. C **3**, 5109 (1970).
[42] *Handbook of Chemistry and Physics,* 69th ed., edited by R. Weast (CRC, Boca Raton, 1988).
[43] F. W. Meyer, S. H. Overbury, C. C. Havener, P. A. Zeijlmans van Emmichoven, J. Burgdörfer, and D. M. Zehner, Phys. Rev. A (to be published).
[44] J. Müller and J. Burgdörfer, Phys. Rev. A **43**, 6027 (1991).
[45] J. N. Bardsley (private communication).